Journal of Controlled Release 171 (2013) 216–224

Contents lists available at ScienceDirect

Journal of Controlled Release

journal homepage: www.elsevier.com/locate/jconrel

The nanoparticulation by octaarginine-modified liposome improves α-galactosylceramide-mediated antitumor therapy *via* systemic administration

Takashi Nakamura, Daiki Yamazaki, Jun Yamauchi, Hideyoshi Harashima *

Faculty of Pharmaceutical Sciences, Hokkaido University, Kita 12 Nishi 6, Kita-ku, Sapporo, Hokkaido 060-0812, Japan

ARTICLE INFO

Article history:
Received 1 March 2013
Accepted 7 July 2013
Available online 13 July 2013

Chemical compound studied in this article:
Alpha-galactosylceramide (PubChem CID: 2826713)

Keywords:
Liposome
Cancer immunotherapy
Cell penetrating peptide
Natural killer T cell

ABSTRACT

Alpha-galactosylceramide (αGC), a lipid antigen present on CD1d molecules, is predicted to have clinical applications as a new class of adjuvant, because αGC strongly activates natural killer T (NKT) cells which produce large amounts of IFN-γ. Here, we incorporated αGC into stearylated octaarginine-modified liposomes (R8-Lip), our original delivery system developed for vaccines, and investigated the effect of nanoparticulation. Unexpectedly, the systemic administered R8-Lip incorporating αGC (αGC/R8-Lip) failed to improve the immune responses mediated by αGC compared with soluble αGC *in vivo*, although αGC/R8-Lip drastically enhanced αGC presentation on CD1d in antigen presenting cells *in vitro*. Thus, we optimized the αGC/R8-Lip *in vivo* to overcome this inverse correlation. In optimization *in vivo*, we found that size control of liposome and R8-modification were critical for enhancing the production of IFN-γ. The optimization led to the accumulation of αGC/R8-Lip in the spleen and a positive therapeutic effect against highly malignant B16 melanoma cells. The optimized αGC/R8-Lip also enhanced αGC presentation on CD1d in antigen presenting cells and resulted in an expansion in the population of NKT cells. Herein, we show that R8-Lip is a potent delivery system, and size control and R8-modification in liposomal construction are promising techniques for achieving systemic αGC therapy.

1. Introduction

Alpha-galactosylceramide (αGC) is a unique adjuvant that enables the activation of both specific and non-specific immune responses. In general, adjuvants such as the toll-like receptor ligand activate innate immunity *via* the production of inflammatory cytokines and type I interferon (IFN). On the other hand, αGC activates innate and adaptive immunity *via* the production of large amounts of INF-γ, which would be expected to show antitumor activity independent of the specific class of tumor [1]. αGC, a synthetic glycolipid, is presented by CD1d molecules, antigen-presenting molecules, to invariant natural killer T (NKT) cells [2–4]. NKT cells recognize the resulting αGC/CD1d complex *via* semi-invariant T cell receptors (Vα14-Jα18 in mice; Vα24-Jα18 in humans), resulting in activation. The semi-invariant T cell receptor of NKT cells confers an important advantage in αGC therapy, because there is very little individual difference between T cell receptors, and, because of this, the effect would be similar, irrespective of patient. Thus, it is expected as versatile cancer immune therapy to have an effect on all patients. The therapeutic value of NKT cells was first discovered in studies using αGC in a metastatic tumor model, which prevents the metastasis of intravenously infected B16 melanoma cells in the lungs of mice [2,5]. This protection activity is dependent on the production of large amounts of INF-γ from NKT cells and on the activation of NK cells and killer T cells, but not on the direct effect of NKT cells themselves [6]. Owing to its unique and strong antitumor ability, many pre-clinical and clinical studies of αGC as KRN7000 were initiated. KRN7000, which is now in clinical trials, contains sucrose, L-histidine and Tween20 as a dispersant. The clinical responses varied, depending on the therapeutic approach used, such as the direct injection of αGC and cell therapies using DC or NKT cells [7]. Although an intravenous administration of soluble αGC did not result in measurable clinical benefits, the intravenous injection of αGC-loaded dendritic cells (DCs) led to an increase in serum levels of IL-12 and IFN-γ and an expansion of the NKT cell population in lung cancer and head and neck cancer patients [8–12]. In other words, while αGC has few effects in *in vivo* direct treatments, it appears to be effective in *ex vivo* cell therapies. These results clearly suggest that soluble αGC is not taken up efficiently by antigen presenting cells (APCs). Hence, to induce a sufficient immune response by the systemic administration of αGC, it will be necessary to control the disposition and cellular uptake of αGC with the currently available delivery systems. In addition, development of delivery systems which achieve

* Corresponding author at: Faculty of Pharmaceutical Sciences, Hokkaido University, Kita 12 Nishi 6, Sapporo City, Hokkaido 060-0812, Japan. Tel.: +81 11 706 3919; fax: +81 11 706 4879.
E-mail address: harasima@pharm.hokudai.ac.jp (H. Harashima).

0168-3659
http://dx.doi.org/10.1016/j.jconrel.2013.07.004

systemic administration of αGC must contribute for versatile cancer therapy. The therapeutic effects of DC therapy using αGC are dependent on the accession efficiency of administered DCs, that is, applications of DC therapy against diseases, other than lung cancer and head and neck cancer, would likely be difficult. On the other hand, it is expected that delivery systems that involve the systemic administration of αGC will be applicable to diseases other than lung cancer and head and neck cancer, because the delivery systems could be used to control the tissue distribution of αGC.

In a previous study, we reported on the potential of stearylated octaarginine-modified liposomes (R8-Lip) as a vaccine delivery system [13–16]. Octaarginine (R8) is a cell-penetrating peptide (CPP). CPPs can be useful for delivering various molecules to cells [17]. The R8 peptide was conjugated with a stearyl moiety and the resulting stearylated R8 (STR-R8) was attached to the liposomal surface, a process that permitted the flexibility and function of the R8 peptide to be maintained [18,19]. R8-Lip in which ovalbumin is encapsulated as a protein antigen, was efficiently taken up by dendritic cells (DCs) and induced strong antigen presentation *via* MHC class I molecules *in vitro*, suggesting that R8-Lip has the potential for serving as a potent carrier for delivering antigens to DCs [13]. In addition to protein antigens, we also reported on the efficient delivery of lipid antigens, such as glucose monomycolate and glycerol monomycolate, and the induction of immune responses *via* CD1 antigen presentation after subcutaneous injection *in vivo* [15,16]. Although we have generally demonstrated the utility of R8-Lip as a vaccine delivery system for the *in vitro* targeting of DCs and subcutaneous immunization, an application of R8-Lip for systemic immunization, the issue of whether it can be used in systemic immunization, namely intravenous administration has not been addressed. Moreover, very few studies have been devoted to examining adjuvant effects of αGC by incorporating αGC into delivery systems [20–22]. In particular, the effect of liposomal αGC against tumors and the mechanism responsible for the immune responses mediated by liposomal αGC remain unverified.

In this study, we incorporated αGC into R8-Lip and investigated the potential of R8-Lip as a delivery system for αGC therapy *via* a systemic treatment. In *in vitro* experiments, we confirmed the efficiency of αGC presentation on CD1d molecules in JAWSII cells, a cell line of murine DCs. In *in vivo* experiments, optimization of the R8-Lip incorporating αGC (αGC/R8-Lip) was performed to control the biodistribution of the R8-Lip, especially for spleen targeting, based on the production of IFN-γ in serum. The therapeutic effect of the optimized αGC/R8-Lip against lung metastasis was then examined in highly malignant B16 melanoma cells. To confirm that the immune responses caused by αGC/R8-Lip occurred *via* αGC machinery, we also investigated αGC presentation on CD1d in APCs and the NKT population after the systemic administration of αGC/R8-Lip. The findings reported herein indicate that the nanoparticulation of αGC by R8-Lip drastically enhanced immune responses *via* the αGC machinery, when the materials were systemically administered.

2. Materials and methods

2.1. Materials

Egg phosphatidylcholine (EPC) and N-(Carbonyl-methoxypolyethyleneglycol 2000)-1,2-distearoyl-sn-glycero-3-phosphoethanolamine (DSPE-PEG2000) were purchased from NOF Corporation (Tokyo, Japan). Cholesterol (Chol) was purchased from AVANTI Polar Lipids Inc. (Alabaster, AL, USA). STR-R8 was synthesized by KURABO (Osaka, Japan). αGC (KRN7000) was obtained from Funakoshi Co. Ltd. (Tokyo, Japan). [^{3}H] cholesteryl hexadecyl ether (CHE) was purchased from PerkinElmer Co. Ltd. (Waltham, MA, USA). Anti-mouse alpha GalCer:CD1d Complex PE was purchased from eBioscience (San Diego, CA, USA). Alexa Fluor 647 anti-mouse I-A/I-E, PE/Cy7 anti-mouse CD19, FITC anti-mouse CD3 and each of the isotype controls were obtained from BioLegend (San Diego, CA, USA). Mouse CD1d Tetramer-SA-PE was purchased from MBL International (Woburn, MA, USA).

2.2. Cells and animals

JAWSII cells derived from murine dendritic cells were purchased from the American Type Culture Collection (Manassas, VA). JAWSII cell was cultured by α-MEM (SIGMA-Aldrich, St. Louis, MO) containing 20% FBS, 100 U/ml penicillin-streptomycin, 4 mmol/l L-grutamine, 1 mmol/l sodium pyruvate and 5 ng/ml GM-CSF. B16-F10 murine melanoma cells stably expressing luciferase (GL4) (B16-F10-luc2; Caliper Life Sciences, MA, USA) were grown in 10% FBS in RPMI-1640 (SIGMA-Aldrich, St. Louis, MO). C57BL/6 (H-2b) female mice (6 to 8 weeks old) were obtained from Japan SLC, Inc. (Shizuoka, Japan). Experiments using mice were approved by the Pharmaceutical Science Animal Committee of Hokkaido University.

2.3. Preparation of liposomes incorporating αGC

Liposomes were composed of EPC, Chol and STR-R8 (70:30:5 molar ratio). DSPE-PEG2000 was included in some cases. 560 nmol of EPC, 240 nmol of Chol, 40 nmol STR-R8 or/and 8, 16, 40 nmol of DSPE-PEG2000 in chloroform solutions were initially mixed in a test tube and 100 μg (117 nmol) of αGC was then added. The solvent was removed with a stream of nitrogen to produce a lipid film. 0.2 ml of 10 mmol/l HEPES (pH 7.4) was added to the lipid film, and the mixture was incubated for 30 min at room temperature to hydrate the film. The hydrated lipid film was then mixed to produce liposomes. The liposome suspension was extruded through polycarbonate membrane filters (400-nm, 800-nm or 1000-nm pore size; Nucleopore) with a Mini-Extruder (Avanti Polar Lipids Inc., Alabaster, AL, USA) for sizing of liposomes. In the case of αGC/R8-Lip (unoptimized), the liposome suspension was sonicated in a bath type sonicator instead of using an extrusion step. The solutions after extrusion or sonication were used as liposome samples. These liposomes are used for experiments within 2 days of their preparation. The concentrations of lipid were determined by means of a phospholipid assay kit (Wako, Osaka, Japan). The lipid concentration of liposomes without extrusion was 3.9 mM, while the lipid concentration and yield of extruded liposomes were 2.1 mM and 61%, respectively. The incorporation ratio of αGC into a liposome is considered to be 100%, because αGC appears to act as a lipid (EPC and Chol). The αGC concentrations in liposome solutions were calculated from the phospholipid concentration. The αGC concentrations of liposomes without or with extrusion were calculated to be 0.48 mg/ml and 0.26 mg/ml, respectively. The diameter of the liposomes was measured by dynamic light scattering, and zeta potentials were determined by laser-Doppler velocimetry with a ZETASIZER Nano (ZEN3600, Malvern Instruments Ltd., Malvern, WR, UK).

2.4. αGC presentation on CD1d in JAWSII cell

2×10^5 JAWSII cells were cultured in a 6-well plate for 48 h. The cells were washed with phosphate buffer saline (PBS), and the medium was then replaced with 1 ml of serum-free medium containing αGC/R8-Lip or soluble αGC. Soluble αGC is prepared as a solution of 1 mg/ml in 100% DMSO with heating at 80 °C for several minutes. The solution of 1 mg/ml in DMSO was diluted to more than 100 times with medium. The final concentration of DMSO in the medium was less than 1%. The cells were then incubated for 3 h. Thereafter, the medium was replaced with fresh medium containing 20% serum, and incubated for an additional 21 h. After the incubation, the cells were washed with PBS and collected into tubes. The cells were stained with anti-mouse alpha GalCer:CD1d Complex PE. The fluorescence of stained cells was measured by FACSCalibur (BD Biosciences).

2.5. Measurement of IFN-γ in serum

C57BL/6 mice were intravenously injected with each sample equivalent to 5 μg of αGC into the tail. Soluble αGC was prepared by dissolving in PBS containing 5.6% sucrose, 0.75% L-histidine and 0.5% Tween20 with heating at 80 °C for several minutes. The volume injected was 200 μl. After 18 h, blood samples were collected from the heart using needle and syringe. After allowing the blood to clot, the samples were centrifuged. The supernatants were used as serum samples. IFN-γ level in serum was measured by an ELISA kit (R&D systems, Basel, Switzerland). These experiments were carried out following the manufacturer's instructions.

2.6. Pharmacokinetic analysis of the liposomes

0.25 nmol of cholesteryl hexadecyl ether, [cholesteryl-1,2-^{3}H(N)]-([^{3}H] CHE, 40 Ci/mmol) was added, when lipid film was prepared. The amount of [^{3}H] CHE was 0.03 mol% of total lipids. Liposomes including [^{3}H] CHE were injected into the tail vein of C57BL/6 mice at a dose of 5 μg αGC. Injected volume was 200 μl. The mice were sacrificed 10, 30 and 90 min after the injection and blood, lung, liver and spleen were collected. To determine the actual uptake of liposomes in tissues, the liposomes in the vascular space was removed by perfusion. After weighing the samples, they were dissolved in Soluene-350 (PerkinElmer, Waltham, MA, USA) overnight at 50 °C. The radioactivities of the samples were determined by liquid scintillation counting, after adding 10 ml of scintillation fluid (Hionic Fluor, PerkinElmer, Waltham, MA, USA).

2.7. Anti-tumor effects in lung metastatic tumor models

On day 0, 2×10^5 cells of B16-F10-luc2 in 200 μl of PBS were injected into the tail vein of C57BL/6 mice. On day 4, soluble αGC and liposome (injected volume: 200 μl) were intravenously injected at a dose of 5 μg αGC into the tail. Soluble αGC was prepared as described in Section 2.5. On day 19, the mice were sacrificed, and the lungs were collected. For the quantification of tumor metastasis, the collected lungs were completely homogenized using a POLYTRON homogenizer (KINEMATICA, Littan, Switzerland) in 1 ml of lysis buffer (100 mM Tris–HCl, 2 mM EDTA, 0.1% TritonX-100, pH 7.8). The luciferase activities were then measured using a luminometer (Luminescencer-PSN, ATTO, Japan). Luciferase activities are expressed as relative light units (RLU) per whole lung.

2.8. αGC presentation on CD1d in antigen presenting cells in vivo

Soluble αGC and liposome (injected volume: 200 μl) were intravenously injected at a dose of 5 μg αGC into the tail. Soluble αGC was prepared as described in Section 2.5. After 15 h, the spleens were collected, and splenocytes were prepared. 2×10^6 splenocyte cells were stained by anti-mouse alpha GalCer:CD1d Complex PE and Alexa Fluor 647 anti-mouse I-A/I-E. The fluorescence of stained cells was measured by FACSCalibur (BD Biosciences).

2.9. Population of NKT cells in vivo

Soluble αGC and liposome (injected volume: 200 μl) were intravenously injected at a dose of 5 μg αGC into the tail. Amount of injected liposomes was 40 nmol. Soluble αGC was prepared as described in Section 2.5. After 3 days, the spleens were collected, and splenocytes were isolated. 1×10^7 splenocyte cells were stained by PE/Cy7 anti-mouse CD19, FITC anti-mouse CD3 and mouse CD1d Tetramer-SA-PE. The fluorescence of stained cells was measured by FACSCalibur (BD Biosciences). NKT cell population was identified as CD19$^-$/CD3$^+$/CD1d tetramer$^+$ cells.

2.10. Statistical analysis

Pair-wise comparisons between treatments were made using an unpaired *t*-test. Comparisons between multiple treatments were made by one-way analysis of variance, followed by the Tukey–Kramer test. A P value of <0.05 was considered to be a significant difference.

3. Results

3.1. Efficiencies of αGC presentation on CD1d in JAWSII cells

αGC is presented on CD1d molecules after being taken up by APCs. We first investigated the efficiencies of the antigen presentation of αGC on CD1d by αGC/R8-Lip in JAWSII cells, a cell line of mouse dendritic cells. In this experiment, we used a αGC/R8-Lip preparation that was composed of EPC, Chol and STR-R8 (molar ratio: 70/30/5). The diameter, zeta potential and polydispersity index (PDI) of the αGC/R8-Lip particles were 98 nm, 40 mV and 0.204, respectively. The αGC/R8-Lip was pulsed to JAWSII cells. Non-liposomal αGC (soluble αGC) was conventionally prepared by dissolving αGC in DMSO and was used in *in vitro* experiments. The JAWSII cells were

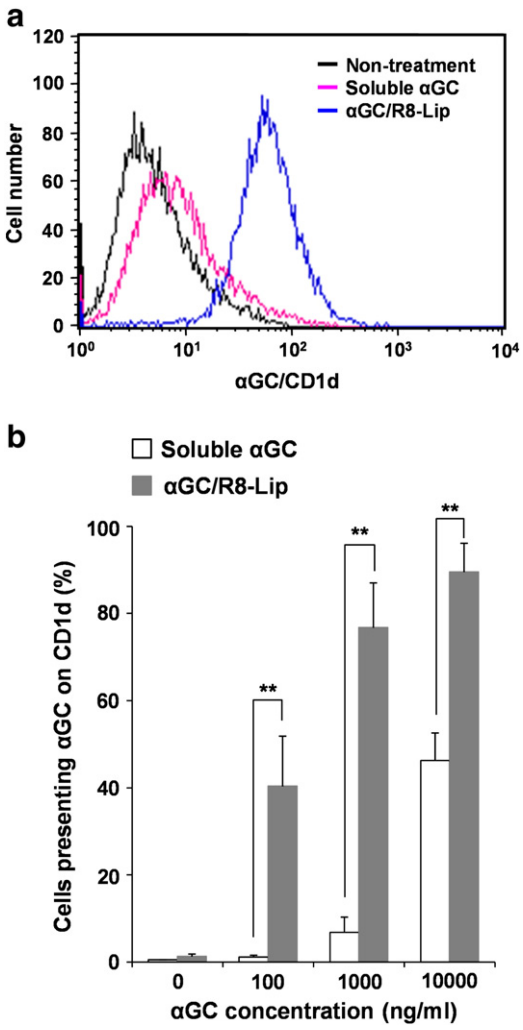

Fig. 1. Presentation of α-galactosylceramide (αGC) *via* CD1d molecules in JAWSII cells. JAWSII cells were cultured with soluble αGC or octaarginine-modified liposome incorporating αGC (αGC/R8-Lip). After 24 h, the cells were collected and stained with an anti-αGC:CD1d antibody. The stained cells were analyzed by flow cytometry. (a) Typical histograms of non-treated cells (black), soluble αGC treated cells (pink) and αGC/R8-Lip treated cells (blue) at a dose of 1000 ng/ml αGC. (b) The percent of anti-αGC/CD1d positive cells at several doses of αGC. Values are the mean ± SD of at least three different experiments (**$P < 0.01$).

stained with anti-αGC/CD1d 24 h after pulsing and were analyzed by flow cytometry. As a result, the histogram of cells treated with αGC/R8-Lip was shifted drastically, compared to that of non-treated cells and cells that had been treated with soluble αGC (Fig. 1a). Fig. 1b shows the percent of anti-αGC/CD1d positive cells, namely the percent of cells presenting αGC on CD1d. The αGC presentations induced by the αGC/R8-Lip increased in a dose-dependent manner and were significantly higher than the corresponding values for soluble αGC (Fig. 1b). Moreover, the value of αGC/R8-Lip at 100 ng/ml was comparable to that of soluble αGC at a concentration of 10000 ng/ml, suggesting that the efficiency of αGC presentation by αGC/R8-Lip was 2 orders of magnitude higher in comparison with that of soluble αGC (Fig. 1b). Thus, as shown in Fig. 1, R8-Lip efficiently delivers αGC to APCs and induces a strong αGC presentation on CD1d.

3.2. INF-γ production of αGC/R8-Lip after intravenous administration in vivo

αGC induced the production of IFN-γ from NKT cells *via* CD1d presentation by APCs [2,23]. We next examined the production of IFN-γ after the intravenous administration of αGC/R8-Lip in mice. Mice were intravenously administered soluble αGC or αGC/R8-Lip. After 18 h, serum samples were collected and the concentrations of IFN-γ were determined by ELISA. Unexpectedly, the concentration of IFN-γ after the αGC/R8-Lip treatment was similar to that of soluble αGC (Fig. 2). This result indicates that the mere modification of R8 for efficient cellular internalization is inefficient for enhancing αGC therapy *via* systemic injection.

3.3. Optimization of αGC/R8-Lip in vivo

To overcome the inverse correlation (Fig. 2), we optimized αGC/R8-Lip by controlling the pharmacokinetics of the process, based on the production of IFN-γ *in vivo*. The spleen is a major target tissue for immunization *via* intravenous administration. The surface of the particles was modified with PEG and the size of the liposomes was controlled, in an attempt to improve the action of αGC/R8-Lip. PEG modification leads to the stabilization of liposomes and the suppression of non-specific interactions. In addition, the size of nano particles is an important factor when the spleen is a target for the uptake by APCs [24]. αGC/R8-Lip was modified with DSPE-PEG2000 at 1 mol%, 2 mol% and 5 mol% of the total lipid. The diameter, PDI and zeta-potential were determined to be as follows: 1 mol% of DSPE-PEG2000 (85 nm, 0.219, 29 mV), 2 mol% of DSPE-PEG2000 (99 nm, 0.273, 20 mV), and 5 mol% of DSPE-PEG2000 (94 nm, 0.263, 19 mV). Although 2 mol% of DSPE-PEG2000 modified αGC/R8-Lip (αGC/R8/2%PEG-Lip) resulted in a slight increase in the production of IFN-γ, modification of 1 mol% and 5 mol% of DSPE-PEG2000 to αGC/R8-Lip impaired the production of IFN-γ (Fig. 3a). We next controlled the size of the αGC/R8/2%PEG-Lip by passing the particles through 400-nm, 800-nm and 1000-nm of polycarbonate membrane filters. The sizes of the αGC/R8/2%PEG-Lip particles were 158 nm (400-nm filter; PDI 0.211; 25 mV),

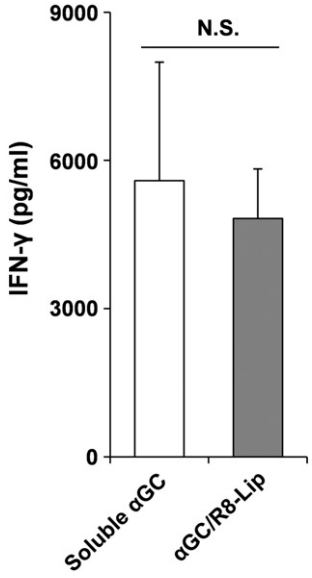

Fig. 2. The production of IFN-γ after intravenous administration of octaarginine-modified liposome incorporating α-galactosylceramide (αGC/R8-Lip). Each sample at a dose of 5 μg αGC was intravenously administered to mice. After 18 h, serum samples were collected and IFN-γ concentrations of sera were measured by ELISA. Values are the mean ± SD (n = 3, N.S.: no significant difference).

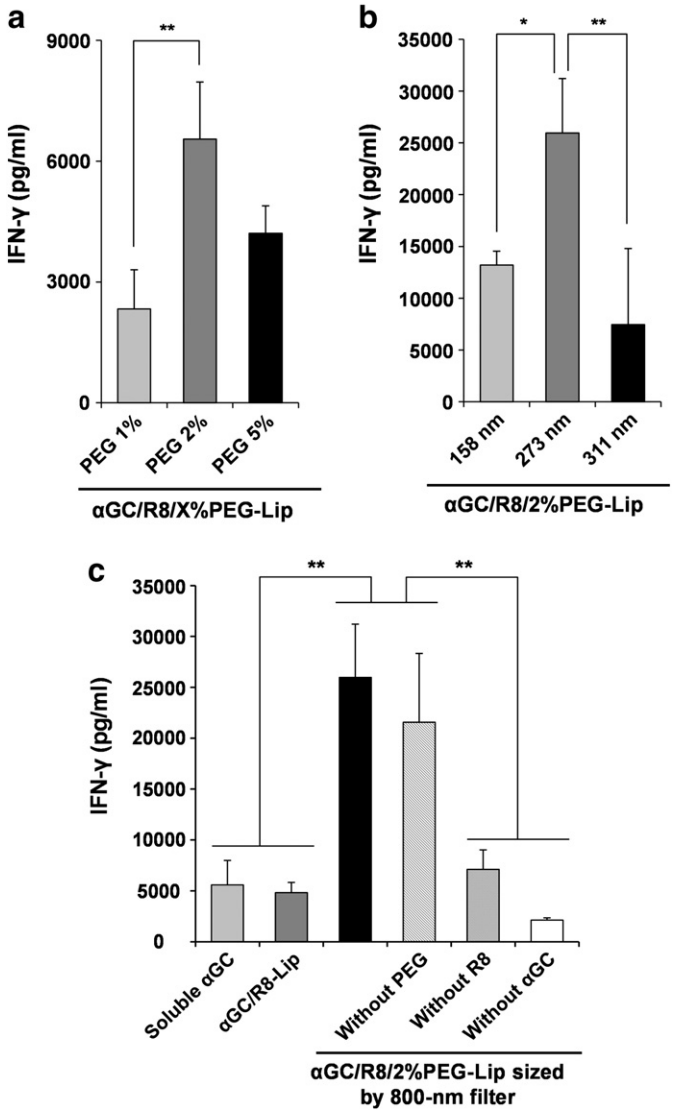

Fig. 3. Optimization of octaarginine-modified liposome incorporating α-galactosylceramide (αGC/R8-Lip). Each sample at a dose of 5 μg αGC was intravenously administered to mice. After 18 h, serum samples were collected and IFN-γ concentrations of sera were measured by ELISA. (a) Optimization of ratio of polyethylene glycol (PEG) modification into αGC/R8-Lip. αGC/R8-Lip was modified with PEG at 1 mol%, 2 mol% and 5 mol% of total lipids. (b) Size effect of R8/2% PEG-modified liposome incorporating αGC (αGC/R8/2%PEG-Lip). The sizes of αGC/R8/2%PEG-Lip were controlled by passage through 400-nm, 800-nm and 1000-nm filters. (c) The production of IFN-γ by optimized αGC/R8-Lip (αGC/R8/2%PEG-Lip sized by 800-nm filter) was compared to those of soluble αGC and unoptimized αGC/R8-Lip. And the effects of PEG, R8 and αGC on the production of IFN-γ were confirmed in the optimized αGC/R8-Lip. Values are the mean ± SD (n = 3–6, *P < 0.05, **P < 0.01).

273 nm (800-nm filter; PDI 0.278; 28 mV) and 311 nm (1000-nm filter; PDI 0.286; 28 mV), respectively. As shown in Fig. 3b, although controlling the size using filters promoted the production of IFN-γ, the αGC/R8/2%PEG-Lip that was sized by the 800-nm filter showed the highest promotion effect. The promotion effect of the αGC/R8/2%PEG-Lip that was sized using an 800-nm filter was more than 5 times greater than that of soluble αGC and the unoptimized αGC/R8-Lip (Fig. 3c). That is, the production of IFN-γ was substantially escalated by optimizing particle diameter by size control. In the case of αGC/R8/PEG-Lip without R8, the production of IFN-γ was significantly decreased, although the αGC/R8/2%PEG-Lip without PEG showed a slightly low value of IFN-γ of αGC/R8/2%PEG-Lip (Fig. 3c). This result indicates that R8 modification also affects to the efficient production of IFN-γ. Consequently, we used the αGC/R8/2%PEG-Lip sized by passage through an 800-nm filter as the optimized αGC/R8-Lip (αGC/R8/PEG-Lip) in subsequent experiments.

3.4. Tissue distribution of αGC/R8-Lip and αGC/R8/PEG-Lip

To determine the influence of optimization in the pharmacokinetics of the process, we examined the tissue distribution of αGC/R8-Lip (unoptimized) and αGC/R8/PEG-Lip (optimized), labeled with [^{3}H] CHE, at 10, 30 and 90 min after intravenous administration, followed by blood perfusion. As shown in Fig. 4a, although αGC/R8-Lip accumulated in the liver in a time-dependent manner, the accumulation of αGC/R8/PEG-Lip in the liver was suppressed and it rapidly accumulated in the spleen. Of note, the fold increase in the accumulation of αGC/R8/PEG-Lip in the spleen, calculated as the organ distribution of αGC/R8/PEG-Lip divided by that of αGC/R8-Lip, was significantly higher compared with other organs (Fig. 4b). Thus, these results show that the αGC/R8/PEG-Lip induced a rapid accumulation in the spleen, suggesting that the rapid accumulation of αGC in the spleen by αGC/R8/PEG-Lip stimulated the production of IFN-γ.

3.5. Antitumor effect of αGC/R8/PEG-Lip against lung metastases model

We then investigated the antitumor effect of αGC/R8/PEG-Lip against B16 melanoma cells, a lung metastatic model. Mice were intravenously grafted with 2×10^5 B16-F10-luc cells, a highly malignant and highly metastatic type of melanoma, and soluble αGC and αGC/R8/PEG-Lip were intravenously administered after 4 days (Fig. 5a). As shown in Fig. 5b, no macroscopic antitumor effects were observed in the lungs of the soluble αGC treated group. On the other hand, the treatment of αGC/R8/PEG-Lip clearly inhibited lung metastasis (Fig. 5b). In addition to the macroscopic observations, the amount of lung metastasis was quantitatively examined by measuring luciferase activities in the lung. No significant antitumor effect was observed in the soluble αGC treated group compared to the non-treatment group (Fig. 5c). To the contrary, αGC/R8/PEG-Lip treatment significantly inhibited lung metastasis in comparison with non-treatment and the treatment with soluble αGC (Fig. 5c). The inhibition effect of lung metastasis in the αGC/R8/PEG-Lip treated group was more than 65% (Fig. 5c). Therefore, these findings suggest that αGC/R8/PEG-Lip has antitumor effects against lung metastasis mediated by a highly malignant melanoma.

3.6. αGC/R8/PEG-Lip enhances αGC presentation on CD1d in APCs in vivo

We examined the issue of whether αGC presentation on CD1d was promoted by an *in vivo* αGC/R8/PEG-Lip treatment. Mice were intravenously treated with soluble αGC or αGC/R8/PEG-Lip and the splenocytes were stained by anti-major histocompatibility complex (MHC) class II and anti-αGC/CD1d antibodies after 15 h. Fig. 6a shows typical dot plots for each group. The area in the upper right shows the distribution of cells stained by both anti-MHC class II and anti-αGC/CD1d antibodies. The values were subtracted from the values

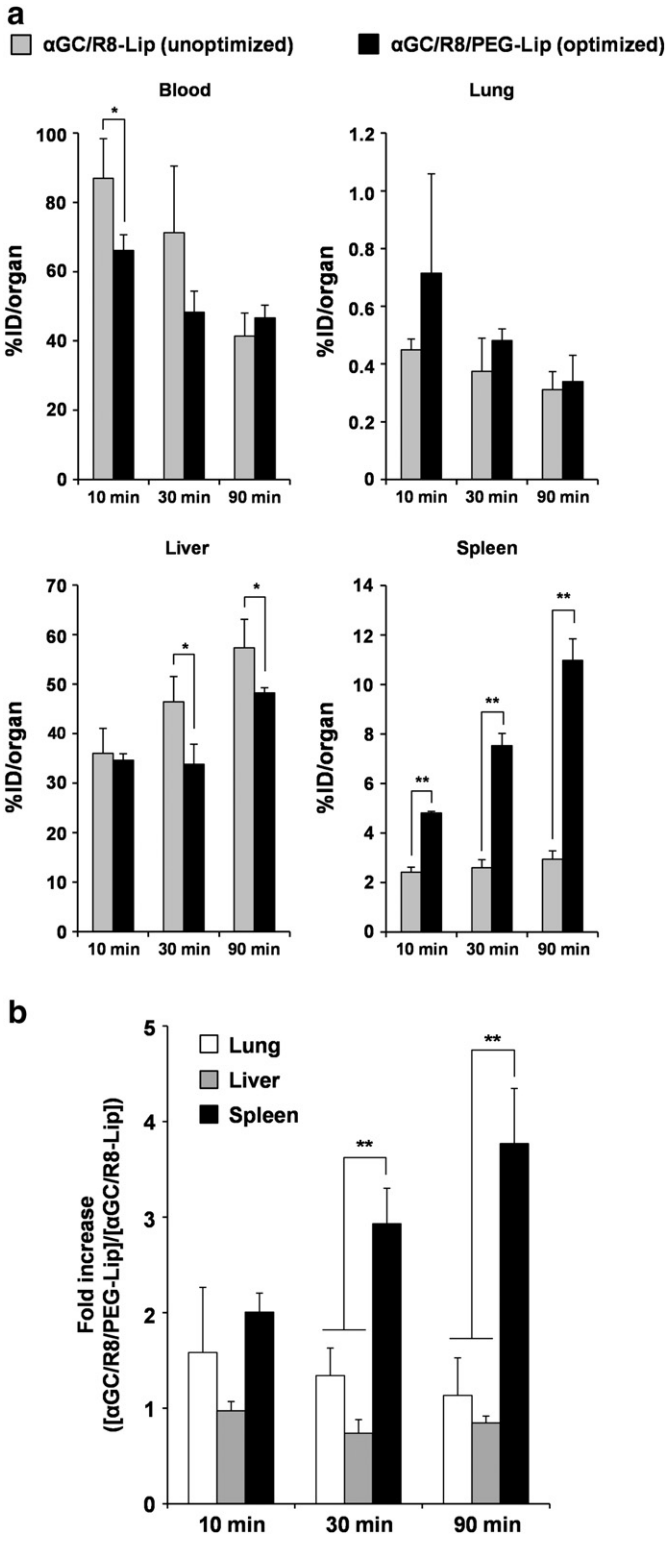

Fig. 4. The biodistribution of octaarginine-modified liposome incorporating α-galactosylceramide (αGC/R8-Lip, unoptimized) and R8/2% polyethylene glycol modified liposome incorporating αGC (αGC/R8/PEG-Lip, optimized). αGC/R8-Lip and αGC/R8/PEG-Lip labeled with [^{3}H] CHE were injected intravenously into mice. After 10, 30 and 90 min, the mice were sacrificed and the distributions of the liposomes were evaluated. Biodistribution is expressed as the percentage of the injected dose per organ (%ID/organ). (a) Blood, lung, liver and spleen. (b) The fold increase of optimization is expressed as the organ distribution of αGC/R8/PEG-Lip per that of αGC/R8-Lip (αGC/R8/PEG-Lip/αGC/R8-Lip). Values are the mean ± SD (n = 3, *P < 0.05, **P < 0.01).

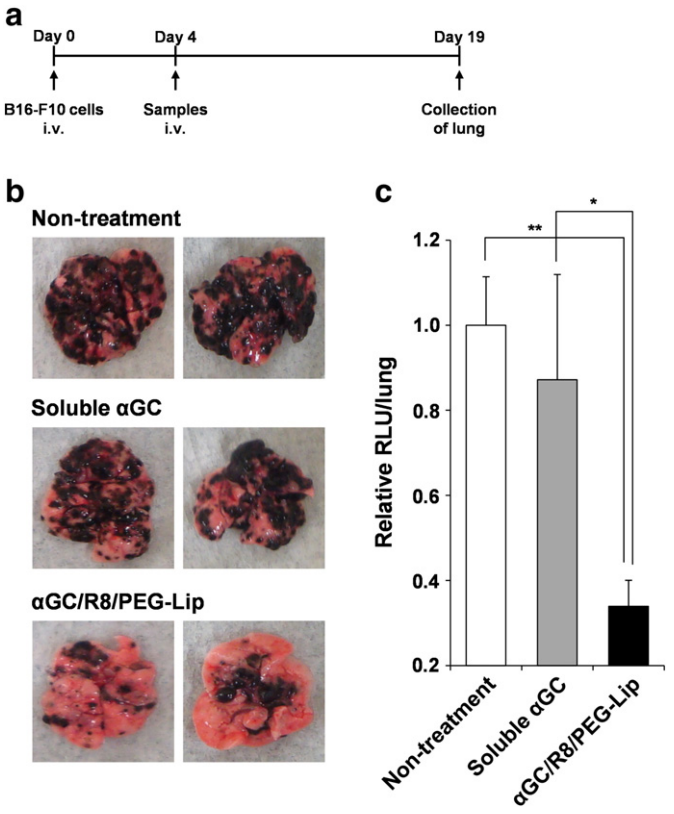

Fig. 5. Therapeutic effects on experimental lung metastasis model with B16-F10 melanoma. (a) Experimental scheme. B16-F10 melanoma cells stably expressing luciferase (B16-F10-luc2) were intravenously inoculated to mice. After 4 days, soluble α-galactosylceramide (αGC) or octaarginine/2% polyethylene glycol-modified liposome incorporating αGC, which was passed through 800 nm filter (αGC/R8/PEG-Lip) were intravenously injected at a dose of 5 μg αGC. On day 19, the lungs were collected. (b) Pictures of the lungs collected on day 19. (c) Quantitative analysis of lung metastasis by measuring luciferase activities. For the quantification of tumor metastasis, the collected lungs were completely homogenized and the luciferase activities were then measured. Luciferase activities are expressed as relative light units (RLU) per whole lung. Values are the mean ± SD (n = 5–7, *P < 0.05, **P < 0.01).

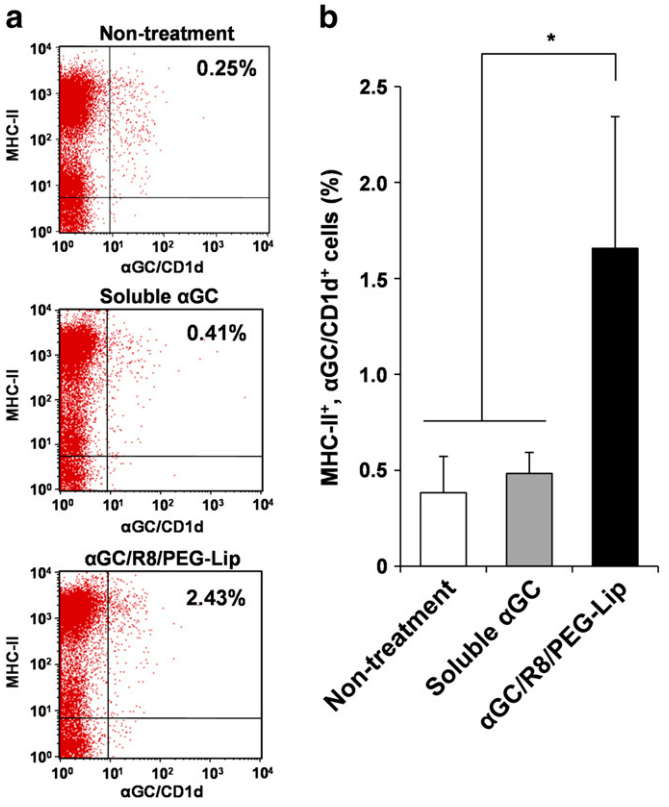

Fig. 6. Antigen presentation of α-galactosylceramide (αGC) on CD1d molecules in antigen presenting cells (APCs). Mice were intravenously administered soluble αGC or octaarginine/2% polyethylene glycol-modified liposome incorporating αGC, which was passed through an 800 nm filter (αGC/R8/PEG-Lip) at a dose of 5 μg αGC. After 18 h, the spleens were collected and the single cell suspensions of splenocyte were prepared. The cell suspensions were then stained by anti-MHC class II (MHC-II) antibody (Alexa Fluor 647) and anti-alpha GalCer:CD1d Complex antibody (phycoerythrin) and were analyzed by flow cytometer. APCs presenting αGC on CD1d were identified as MHC-II$^+$/GalCer:CD1d$^+$ cells. (a) Typical dot plots of the splenocyte derived from non-treated mouse, soluble αGC treated mouse and αGC/R8/PEG-Lip treated mouse. The numbers in the upper right area indicate the percentage of MHC-II$^+$/GalCer:CD1d$^+$ cells. (b) The percentages of anti-αGC/CD1d positive cells. Values are the mean ± SD (n = 3, *P < 0.05).

of each isotype control from the values of each sample. In the αGC/R8/PEG-Lip treated group, a significantly increased number of cells were stained by anti-MHC class II and anti-αGC/CD1d, although the soluble αGC treated group was not (Fig. 6b). Hence, this suggests that αGC/R8/PEG-Lip enhances αGC presentation on CD1d in APCs *in vivo*.

3.7. Intravenous administration of αGC/R8/PEG-Lip increases the population of NKT cells in vivo

Lastly, we confirmed that a population of NKT cells was located in the spleen after the administration of soluble αGC or αGC/R8/PEG-Lip. After NKT cells recognized the αGC/CD1d complex on APCs *via* T cell receptors, the NKT cells activate and proliferate. It has been reported to occur rapidly (8–24 h) after the administration of αGC and NKT cells can no longer be detected by tetramer staining. The NKT cells then expanded, reaching maximal levels at 3 days [25]. Mice were intravenously treated with soluble αGC or αGC/R8/PEG-Lip and splenocytes were obtained and stained by an anti-CD19 antibody, an anti-CD3 antibody and a CD1d tetramer after 3 days. The NKT cell population was identified as CD19$^-$/CD3$^+$/CD1d tetramer$^+$ cells. Fig. 7a shows typical dot plots for each. The numbers in the upper right area in Fig. 7a indicate the percentage of CD3$^+$/CD1d tetramer$^+$ cells among the CD19$^-$ cells. The values are subtracted from the values of each isotype control from the values of each sample. The NKT populations in αGC/R8/PEG-Lip treated groups were drastically higher than the corresponding values for the non treated group and the soluble αGC treated groups (Fig. 7b). These data confirm that αGC/R8/PEG-Lip treatment efficiently expanded the population of NKT cells. Meanwhile, the results shown in Figs. 6 and 7 indicate that αGC/R8/PEG-Lip induces immune responses *via* a αGC-mediated mechanism.

4. Discussion

As noted in the introduction, the purpose of the present study was to evaluate the potential for the use of R8-Lip as a delivery system for αGC to achieve efficient αGC therapy *via* systemic administration. Although very few reports have been devoted to investigating the adjuvant effects of αGC by using delivery systems, particularly liposomes [20–22], the enhancement of adjuvant effects of αGC by using liposomes is clearly demonstrated in this study. This is the first report to show the antitumor effect of αGC incorporated liposomes against a B16 lung metastatic model.

We first showed that the αGC/R8-Lip preparation induced a significantly higher αGC antigen presentation on CD1d in JAWSII cells than soluble αGC (Fig. 1). αGC is presented on CD1d in endosomes and lysosomes after internalization by APCs [26]. We hypothesized that this is achieved by the efficient cellular uptake and control of intracellular trafficking aided by αGC/R8-Lip. The surface of the αGC/R8-Lip liposomes was modified with STR-R8. Several reports have

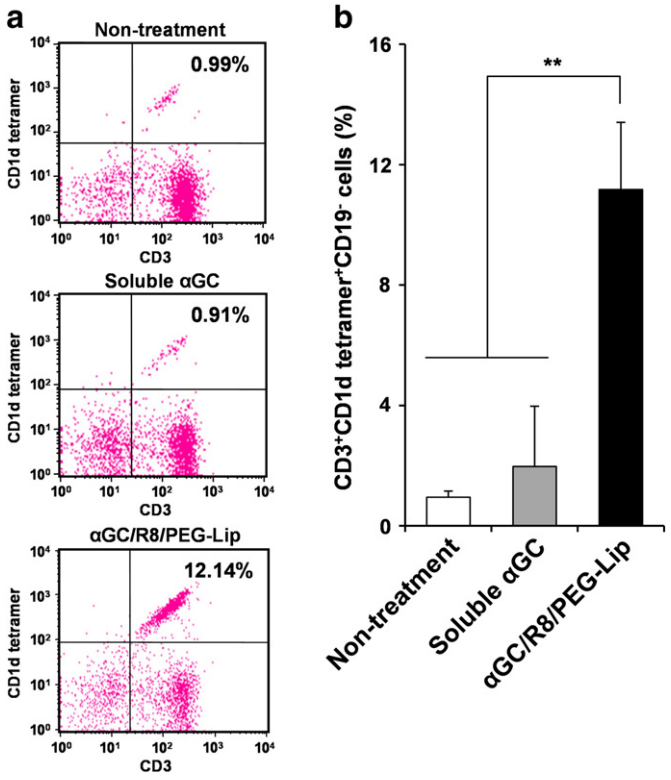

Fig. 7. Population of natural killer T (NKT) cells in the spleen after administration of octaarginine/2% polyethylene glycol-modified liposome incorporating α-galactosylceramide, which was passed through 800 nm filter (αGC/R8/PEG-Lip). Mice were intravenously administered soluble αGC or αGC/R8/PEG-Lip at a dose of 5 μg αGC. After 3 days, the spleens were collected and the single cell suspensions of splenocytes were prepared. The cell suspensions were then stained with an anti-CD19 antibody (PE/Cy7), anti-CD3 antibody (FITC) and CD1d tetramer (PE), and were analyzed by flow cytometry. NKT cell population was identified as $CD19^{-}/CD3^{+}$/CD1d $tetramer^{+}$ cells. (a) Typical dot plots of the splenocyte derived from non-treated mouse, soluble αGC treated mouse and αGC/R8/PEG-Lip treated mouse. The numbers in the upper right area indicate the percentage of $CD3^{+}$/CD1d $tetramer^{+}$ cells among the $CD19^{-}$ cells. (b) The percentages of $CD19^{-}/CD3^{+}$/CD1d $tetramer^{+}$ cells. Values are the mean ± SD (n = 3, $^{**}P < 0.01$).

indicated that when the liposomal surface is modified with STR-R8, cellular internalization is drastically enhanced [13,15,19]. In the case of αGC, the R8-Lip was also efficiently delivered to APCs. Another point is to control the intracellular trafficking of liposomes. CD1d molecules bind to lipid antigens in endosomes and lysosomes. The CD1d molecules that contain bound lipid antigens are then delivered to the cellular membrane and the CD1d molecules present the lipid antigens to NKT cells. The αGC needs to be released from liposomes and to be present in endosomes and lysosomes, and we used EPC and Chol in preparing all liposomes in which αGC was incorporated in this study. The intracellular trafficking of a cargo in a liposome can be controlled by using different lipids. In the case of liposomes containing EPC and Chol, less fusion occurs with the endosomal or lysosomal membranes. As a result, the liposomes remain in the endosomes and lysosomes [15,27]. On the other hand, dioleoyl phosphatidyl ethanolamine (DOPE)-based liposomes were frequently used for escaping from endosomes and delivering cargoes to the cytosol [13,28–30]. We also compared the EPC/Chol based liposome with a fusogenic liposome that was composed of DOPE in αGC presentation on CD1d of JAWSII cells. As a result, the efficiency of αGC presentation by the DOPE-based liposome was enormously lower than that of EPC/Chol-based liposome (data not shown). Consequently, this suggests that αGC/R8-Lip efficiently induces αGC presentation on CD1d in comparison with soluble αGC.

Contrary to our expectations, the production of IFN-γ in mice that had been treated with αGC/R8-Lip was similar to that in mice that had been treated with soluble αGC (Fig. 2). That is, no nanoparticulation effect was observed *in vivo*. This result indicates that it is insufficient to merely incorporate αGC into CPP-modified liposome, such as R8-Lip, to enhance immune response mediated by αGC after systemic injection. In general, liposomes with diameters in the sub-100 nm range have been used for controlling the biodistribution of drugs, because the sub-100 nm size of liposomes decreases recognition by the reticuloendothelial system and the immune system including APCs [31]. The size of the αGC/R8-Lip particles was less than 100 nm. It appears that the αGC/R8-Lip is recognized with difficulty by APCs. As another reason, soluble αGC may form a micelle structure, because soluble αGC used in the *in vivo* experiments contains Tween20, a detergent. Hence, the effect of nanoparticulation might be a factor in the case of soluble αGC, and, as a result, the production of IFN-γ between αGC/R8-Lip and soluble αGC could be comparable. From the results shown in Fig. 2, we optimized the αGC/R8-Lip to promote targeting to the spleen. The spleen is a major target lymphatic organ for immunization *via* intravenous administration and contains high levels of APCs. As a result, αGC/R8/PEG-Lip the size of which was around 270 nm induced a significantly higher level of production of IFN-γ than αGC/R8-Lip or soluble αGC (Fig. 3c). In a previous report, we showed that large sized liposomes (300 nm) accumulate more efficiently in the spleen compared to small sized liposomes (100 nm) [24]. In this study, αGC/R8/PEG-Lip accumulated at much higher levels in the spleen compared to αGC/R8-Lip (Fig. 4). Consequently, the efficiency of delivering αGC to APCs might be enhanced by αGC/R8/PEG-Lip. We also discuss about relationship between particle size and cellular uptake by APCs. APCs such as DCs and macrophages have a unique uptake mechanism, termed phagocytosis. Phagocytosis is an actin-dependent process that involves internalizing particles with sizes in excess of 0.5 μm [32]. Moreover, the macropinocytosis of DCs is also unique. Macropinocytosis is a process of "cell drinking" involving the eruption of membrane ruffles from cell surface, which internalizes particles with sizes up to 5 μm [32,33]. Although macropinocytosis occurs in all cells as the result of some stimulation, macropinocytosis constitutively occurs in DCs in contrast to other cell types [33]. Namely, APCs have a mechanism for the internalization of large particles (>100 nm) and this mechanism is different from that of normal cells. However, the relation between liposome size and the efficiency of cellular uptake by APCs was inconsistent [34]. The suitable size seems to be different depending on the lipid composition, dose, strain, *etc.* In our optimization of the size of αGC/R8/PEG-Lip, particularly, αGC/R8/PEG-Lip prepared using 800-nm of polycarbonate membrane filters, we observed a high production of IFN-γ (Fig. 3c). On the other hand, although the difference in liposome size between 800-nm and 1000-nm filtered liposomes was small (273 nm and 311 nm), the difference in IFN-γ production was large (Fig. 3b). As mentioned above, APCs may be able to take up both types of liposomes *via* macropinocytosis. However, one report indicates that the efficiency of cellular uptake of latex particles by dendritic cells (DCs) starts to decrease from 300 to 400 nm [35]. Thus, the uptake efficiency of liposomes into DCs was possibly different between 273 nm-sized liposomes and 311 nm-sized liposomes. As a result, the small difference in liposomal size may have affected the extent of IFN-γ production in this study. The importance of R8 modification was also shown in Fig. 3c. These data are entirely consistent with our previous reports showing that R8-Lip is a potent vaccine delivery system for lipid antigen presentation and an anti-tumor vaccine *in vivo* [13–16]. We thus conclude that R8-Lip is also useful for αGC delivery. Contrary to R8 modification, PEG modification resulted in a slight enhancement in the production of IFN-γ. Although the findings suggest that PEG modification had some benefit because the optimal value of modification was present (Fig. 3a), further research will clearly be needed in this area.

In *in vivo* animal studies, αGC showed antitumor effects against various tumors in hepatic and lung metastasis models. However, it was no longer effective when treatment with soluble αGC started 3 days after the injection of melanoma cells [36,37]. In our study,

soluble αGC, which was injected 4 days after melanoma cell injection, showed no effect against lung metastasis (Fig. 5). To circumvent this problem, αGC-loaded-DCs were used [7,38,39]. Treatment with αGC-loaded-DCs efficiently inhibited melanoma metastasis, even when the αGC-loaded-DCs were injected 7 days after injection of the melanoma cells [38]. However, several administrations were also necessary in the case of αGC-loaded-DCs. In contrast, the αGC/R8/PEG-Lip effectively inhibited the lung metastasis of melanoma with only one injection 4 days after melanoma cell injection (Fig. 5). In addition, we used B16-F10 cells as model tumor cells for lung metastasis. B16-BL6 cells have been used in a large number of studies. B16-F10 cells were established by 10 successive selections for lung metastasis following intravenous injection [40]. B16-BL6 cells were established from B16-F10 cells that penetrated the mouse bladder membranes [41]. Although B16-F10 and B16-BL6 cells are both malignant and have similar characteristics, when the cells are intravenously injected, the metastasis foci are reported to be greater in the case of B16-F10 than in B16-BL6 [41,42]. Based on this fact, it appears that B16-F10 more effectively establishes metastasis. Therefore, we concluded that the nanoparticulation of αGC with αGC/R8/PEG-Lip drastically improved the anti-metastatic ability of GC.

NKT cells have been shown to play an important role in antitumor immune responses. The antitumor effects of αGC are crucially dependent on NKT cells, because no antitumor effects are observed in NKT cell deficient mice. Immune responses mediated by αGC initiate αGC presentation on CD1d of APCs. NKT cells then recognize αGC on the CD1d of APCs *via* T cell receptors and speedily produce large amounts of IFN-γ [4]. These activated NKT cells then expand, reaching maximal levels at 3 days. Thus, we confirmed αGC presentation on the CD1d of APCs and the expansion of NKT cells which were critical steps in the immune responses mediated by αGC. αGC/R8/PEG-Lip significantly enhanced αGC presentation on the CD1d of APCs and the expansion of NKT cells after intravenous administration (Figs. 6 and 7). The results confirm that the nanoparticulated αGC, αGC/R8/PEG-Lip in this study, can also activate NKT cells in the general manner of αGC-mediated immune responses, and can enhance each process of the αGC-mediated immune responses. The findings that the nanoparticulation of αGC drastically enhances immune responses mediated by αGC *via* activation of NKT cells may be helpful information to develop delivery systems incorporating αGC.

The findings reported herein show that the nanoparticulation of αGC with αGC/R8/PEG-Lip significantly enhanced the presentation of αGC on the CD1d of APCs, the production of IFN-γ and expansion of NKT cells, leading to effective anti-metastatic effect in a highly malignant lung metastasis model, after intravenous administration. We also revealed that the size control and R8-modification in liposomal construction are promising techniques for systemic αGC therapy. Hence, we conclude that αGC/R8/PEG-Lip can function as a potent delivery system for αGC therapy *via* systemic treatment.

Acknowledgments

This work was supported in part by Grant-in-aid for Scientific Research (S) and Grant-in-Aid for Young Scientists (B) from the Ministry of Education, Culture, Sports, Science and Technology of Japan. No potential conflicts of interest were disclosed. We also appreciate Milton S. Feather for this helpful advice in writing the English manuscript.

References

[1] M. Taniguchi, K. Seino, T. Nakayama, The NKT cell system: bridging innate and acquired immunity, Nat. Immunol. 4 (2003) 1164–1165.
[2] T. Kawano, J. Cui, Y. Koezuka, I. Toura, Y. Kaneko, K. Motoki, H. Ueno, R. Nakagawa, H. Sato, E. Kondo, H. Koseki, M. Taniguchi, CD1d-restricted and TCR-mediated activation of valpha14 NKT cells by glycosylceramides, Science 278 (1997) 1626–1629.
[3] M. Exley, J. Garcia, S.P. Balk, S. Porcelli, Requirements for CD1d recognition by human invariant Valpha24+ CD4-CD8- T cells, J. Exp. Med. 186 (1997) 109–120.
[4] V. Cerundolo, J.D. Silk, S.H. Masri, M. Salio, Harnessing invariant NKT cells in vaccination strategies, Nat. Rev. Immunol. 9 (2009) 28–38.
[5] E. Kobayashi, K. Motoki, T. Uchida, H. Fukushima, Y. Koezuka, KRN7000, a novel immunomodulator, and its antitumor activities, Oncol. Res. 7 (1995) 529–534.
[6] J.A. Berzofsky, M. Terabe, The contrasting roles of NKT cells in tumor immunity, Curr. Mol. Med. 9 (2009) 667–672.
[7] J.W. Molling, M. Moreno, H.J. van der Vliet, A.J. van den Eertwegh, R.J. Scheper, B.M. von Blomberg, H.J. Bontkes, Invariant natural killer T cells and immunotherapy of cancer, Clin. Immunol. 129 (2008) 182–194.
[8] G. Giaccone, C.J. Punt, Y. Ando, R. Ruijter, N. Nishi, M. Peters, B.M. von Blomberg, R.J. Scheper, H.J. van der Vliet, A.J. van den Eertwegh, M. Roelvink, J. Beijnen, H. Zwierzina, H.M. Pinedo, A phase I study of the natural killer T-cell ligand alpha-galactosylceramide (KRN7000) in patients with solid tumors, Clin. Cancer Res. 8 (2002) 3702–3709.
[9] F.L. Schneiders, R.J. Scheper, B.M. von Blomberg, A.M. Woltman, H.L. Janssen, A.J. van den Eertwegh, H.M. Verheul, T.D. de Gruijl, H.J. van der Vliet, Clinical experience with alpha-galactosylceramide (KRN7000) in patients with advanced cancer and chronic hepatitis B/C infection, Clin. Immunol. 140 (2011) 130–141.
[10] D.H. Chang, K. Osman, J. Connolly, A. Kukreja, J. Krasovsky, M. Pack, A. Hutchinson, M. Geller, N. Liu, R. Annable, J. Shay, K. Kirchhoff, N. Nishi, Y. Ando, K. Hayashi, H. Hassoun, R.M. Steinman, M.V. Dhodapkar, Sustained expansion of NKT cells and antigen-specific T cells after injection of alpha-galactosyl-ceramide loaded mature dendritic cells in cancer patients, J. Exp. Med. 201 (2005) 1503–1517.
[11] A. Ishikawa, S. Motohashi, E. Ishikawa, H. Fuchida, K. Higashino, M. Otsuji, T. Iizasa, T. Nakayama, M. Taniguchi, T. Fujisawa, A phase I study of alpha-galactosylceramide (KRN7000)-pulsed dendritic cells in patients with advanced and recurrent non-small cell lung cancer, Clin. Cancer Res. 11 (2005) 1910–1917.
[12] S. Motohashi, Y. Okamoto, I. Yoshino, T. Nakayama, Anti-tumor immune responses induced by iNKT cell-based immunotherapy for lung cancer and head and neck cancer, Clin. Immunol. 140 (2011) 167–176.
[13] T. Nakamura, R. Moriguchi, K. Kogure, N. Shastri, H. Harashima, Efficient MHC class I presentation by controlled intracellular trafficking of antigens in octaarginine-modified liposomes, Mol. Ther. 16 (2008) 1507–1514.
[14] T. Nakamura, R. Moriguchi, K. Kogure, H. Harashima, Incorporation of polyinosine-polycytidylic acid enhances cytotoxic T cell activity and antitumor effects by octaarginine-modified liposomes encapsulating antigen, but not by octaarginine-modified antigen complex, Int. J. Pharm. 441 (2013) 476–481.
[15] T. Komori, T. Nakamura, I. Matsunaga, D. Morita, Y. Hattori, H. Kuwata, N. Fujiwara, K. Hiromatsu, H. Harashima, M. Sugita, A microbial glycolipid functions as a new class of target antigen for delayed-type hypersensitivity, J. Biol. Chem. 286 (2011) 16800–16806.
[16] Y. Hattori, I. Matsunaga, T. Komori, T. Urakawa, T. Nakamura, N. Fujiwara, K. Hiromatsu, H. Harashima, M. Sugita, Glycerol monomycolate, a latent tuberculosis-associated mycobacterial lipid, induces eosinophilic hypersensitivity responses in guinea pigs, Biochem. Biophys. Res. Commun. 409 (2011) 304–307.
[17] B. Gupta, T.S. Levchenko, V.P. Torchilin, Intracellular delivery of large molecules and small particles by cell-penetrating proteins and peptides, Adv. Drug Deliv. Rev. 57 (2005) 637–651.
[18] S. Futaki, W. Ohashi, T. Suzuki, M. Niwa, S. Tanaka, K. Ueda, H. Harashima, Y. Sugiura, Stearylated arginine-rich peptides: a new class of transfection systems, Bioconjug. Chem. 12 (2001) 1005–1011.
[19] I.A. Khalil, K. Kogure, S. Futaki, H. Harashima, High density of octaarginine stimulates macropinocytosis leading to efficient intracellular trafficking for gene expression, J. Biol. Chem. 281 (2006) 3544–3551.
[20] A.C. Benoit, Y. Huang, S. Maneewatcharangsri, P. Tapchaisri, R. Anderson, Regulation of airway eosinophil and neutrophil infiltration by alpha-galactosylceramide in a mouse model for respiratory syncytial virus (RSV) vaccine-augmented disease, Vaccine 25 (2007) 7754–7762.
[21] Y. Tamura, A. Teng, R. Nozawa, Y. Takamoto-Matsui, Y. Ishii, Characterization of the immature dendritic cells and cytotoxic cells both expanded after activation of invariant NKT cells with alpha-galactosylceramide *in vivo*, Biochem. Biophys. Res. Commun. 369 (2008) 485–492.
[22] E. Macho Fernandez, J. Chang, J. Fontaine, E. Bialecki, F. Rodriguez, E. Werkmeister, V. Krieger, C. Ehret, B. Heurtault, S. Fournel, B. Frisch, D. Betbeder, C. Faveeuw, F. Trottein, Activation of invariant Natural Killer T lymphocytes in response to the alpha-galactosylceramide analogue KRN7000 encapsulated in PLGA-based nanoparticles and microparticles, Int. J. Pharm. 423 (2012) 45–54.
[23] J.S. Bezbradica, A.K. Stanic, N. Matsuki, H. Bour-Jordan, J.A. Bluestone, J.W. Thomas, D. Unutmaz, L. Van Kaer, S. Joyce, Distinct roles of dendritic cells and B cells in Va14Ja18 natural T cell activation *in vivo*, J. Immunol. 174 (2005) 4696–4705.
[24] K. Takara, H. Hatakeyama, G. Kibria, N. Ohga, K. Hida, H. Harashima, Size-controlled, dual-ligand modified liposomes that target the tumor vasculature show promise for use in drug-resistant cancer therapy, J. Control. Release 162 (2012) 225–232.
[25] V.V. Parekh, M.T. Wilson, D. Olivares-Villagomez, A.K. Singh, L. Wu, C.R. Wang, S. Joyce, L. Van Kaer, Glycolipid antigen induces long-term natural killer T cell anergy in mice, J. Clin. Invest. 115 (2005) 2572–2583.
[26] G. De Libero, L. Mori, Recognition of lipid antigens by T cells, Nat. Rev. Immunol. 5 (2005) 485–496.
[27] A. Homhuan, K. Kogure, H. Akaza, S. Futaki, T. Naka, Y. Fujita, I. Yano, H. Harashima, New packaging method of mycobacterial cell wall using octaarginine-modified

liposomes: enhanced uptake by and immunostimulatory activity of dendritic cells, J. Control. Release 120 (2007) 60–69.
[28] K. Kogure, R. Moriguchi, K. Sasaki, M. Ueno, S. Futaki, H. Harashima, Development of a non-viral multifunctional envelope-type nano device by a novel lipid film hydration method, J. Control. Release 98 (2004) 317–323.
[29] K. Kogure, H. Akita, Y. Yamada, H. Harashima, Multifunctional envelope-type nano device (MEND) as a non-viral gene delivery system, Adv. Drug Deliv. Rev. 60 (2008) 559–571.
[30] H. Akita, K. Kogure, R. Moriguchi, Y. Nakamura, T. Higashi, T. Nakamura, S. Serada, M. Fujimoto, T. Naka, S. Futaki, H. Harashima, Nanoparticles for ex *vivo* siRNA delivery to dendritic cells for cancer vaccines: programmed endosomal escape and dissociation, J. Control. Release 143 (2010) 311–317.
[31] R.T. Proffitt, L.E. Williams, C.A. Presant, G.W. Tin, J.A. Uliana, R.C. Gamble, J.D. Baldeschwieler, Liposomal blockade of the reticuloendothelial system: improved tumor imaging with small unilamellar vesicles, Science 220 (1983) 502–505.
[32] D.M. Underhill, H.S. Goodridge, Information processing during phagocytosis, Nat. Rev. Immunol. 12 (2012) 492–502.
[33] C.C. Norbury, Drinking a lot is good for dendritic cells, Immunology 117 (2006) 443–451.
[34] F. Ahsan, I.P. Rivas, M.A. Khan, A.I. Torres Suarez, Targeting to macrophages: role of physicochemical properties of particulate carriers–liposomes and microspheres–on the phagocytosis by macrophages, J. Control. Release 79 (2002) 29–40.
[35] J.C. Reece, N.J. Vardaxis, J.A. Marshall, S.M. Crowe, P.U. Cameron, Uptake of HIV and latex particles by fresh and cultured dendritic cells and monocytes, Immunol. Cell Biol. 79 (2001) 255–263.
[36] T. Kawano, J. Cui, Y. Koezuka, I. Toura, Y. Kaneko, H. Sato, E. Kondo, M. Harada, H. Koseki, T. Nakayama, Y. Tanaka, M. Taniguchi, Natural killer-like nonspecific tumor cell lysis mediated by specific ligand-activated Valpha14 NKT cells, Proc. Natl. Acad. Sci. U. S. A. 95 (1998) 5690–5693.
[37] M. Taniguchi, M. Harada, S. Kojo, T. Nakayama, H. Wakao, The regulatory role of Valpha14 NKT cells in innate and acquired immune response, Annu. Rev. Immunol. 21 (2003) 483–513.
[38] I. Toura, T. Kawano, Y. Akutsu, T. Nakayama, T. Ochiai, M. Taniguchi, Cutting edge: inhibition of experimental tumor metastasis by dendritic cells pulsed with alpha-galactosylceramide, J. Immunol. 163 (1999) 2387–2391.
[39] S. Fujii, K. Shimizu, M. Kronenberg, R.M. Steinman, Prolonged IFN-gamma-producing NKT response induced with alpha-galactosylceramide-loaded DCs, Nat. Immunol. 3 (2002) 867–874.
[40] I.J. Fidler, Selection of successive tumour lines for metastasis, Nat. New Biol. 242 (1973) 148–149.
[41] G. Poste, J. Doll, I.R. Hart, I.J. Fidler, *In vitro* selection of murine B16 melanoma variants with enhanced tissue-invasive properties, Cancer Res. 40 (1980) 1636–1644.
[42] T. Ishiguro, M. Nakajima, M. Naito, T. Muto, T. Tsuruo, Identification of genes differentially expressed in B16 murine melanoma sublines with different metastatic potentials, Cancer Res. 56 (1996) 875–879.